



**HAL**  
open science

# Global visual saliency: geometric and colorimetric saliency fusion and its applications for 3D colored meshes

Anass Nouri, Christophe Charrier, Olivier Lézoray

► **To cite this version:**

Anass Nouri, Christophe Charrier, Olivier Lézoray. Global visual saliency: geometric and colorimetric saliency fusion and its applications for 3D colored meshes. International Conference on Image Processing, Theory, Tools & Applications (IPTA 2017), Nov 2017, Montréal, Canada. hal-01666354

**HAL Id: hal-01666354**

**<https://hal.science/hal-01666354v1>**

Submitted on 16 Jan 2018

**HAL** is a multi-disciplinary open access archive for the deposit and dissemination of scientific research documents, whether they are published or not. The documents may come from teaching and research institutions in France or abroad, or from public or private research centers.

L'archive ouverte pluridisciplinaire **HAL**, est destinée au dépôt et à la diffusion de documents scientifiques de niveau recherche, publiés ou non, émanant des établissements d'enseignement et de recherche français ou étrangers, des laboratoires publics ou privés.

# Global visual saliency: geometric and colorimetric saliency fusion and its applications for 3D colored meshes

Anass Nouri, Christophe Charrier, Olivier Lézoray  
UNICAEN, ENSICAEN, CNRS, GREYC, Normandie Univ, Caen, France  
anass.nouri@unicaen.fr, christophe.charrier@unicaen.fr, olivier.lezoray@unicaen.fr

**Abstract**—Many computer graphics applications use visual saliency information to guide their treatments such as adaptive compression, viewpoint-selection, segmentation, etc. However, all these applications rest on a partial estimation of visual saliency insofar that only geometric properties of the considered 3D mesh are taken into account leaving aside the colorimetric ones. As humans, our visual attention is sensitive to both geometric and colorimetric informations. Indeed, colorimetric information modifies the eye movements while visualizing a multimedia content. We propose in this paper an innovative approach for the detection of global saliency that takes into account both geometric and colorimetric features of a 3D mesh simulating hence the Human Visual System (HVS). For this, we generate two multi-scale saliency maps based on local geometric and colorimetric patch descriptors. These saliency maps are pooled using the Evidence Theory. We show the contribution and the benefit of our proposed global saliency approach for two applications: automatic optimal viewpoint selection and adaptive denoising of 3D colored meshes.

**Index Terms**—Global saliency, Geometry, Color, 3D colored mesh.

## I. INTRODUCTION

Visual attention represents a major feature of the Human Visual System (HVS) that selects the significative informations in scenes or on objects. When we look to an object, our visual attention is focalized on particular attractive regions rather than on non-interesting ones. These attractive regions are placed in the center of our glance after several eye movements and constitute a restreint part of the visual field that is treated in details by our HVS in contrary to the rest. Many complex attentional mechanisms are involved for selecting these particular regions. We are interested in this paper only on the part of attention related to the saliency of a region.

Visual saliency can be defined as the perceptual information that makes some regions or vertices of a 3D mesh standing out from their surrounding and hence attracts the glance of the human observer. Thereby, the degree of saliency of a region depends on the distinction of the concerned region compared to its neighborhood. This distinction is associated to the geometry or colors of the 3D mesh that represents features

related only to the visual stimuli and not to the observer nor to the task entrusted to him. Hence, the proposed Global Saliency map is more related to the Bottom-up attention process than to the Top-down process.

With the fast development of 3D scanners, we are able from now to scan real objects by acquiring both geometry and colors. The acquired 3D meshes and their computed saliency are used in many computer graphics and computer vision applications such as optimal viewpoint-point selection [1] [2], adaptive mesh simplification [3], face recognition [4], etc. All these applications rest on a partial estimation of visual saliency insofar as only geometric properties of the considered 3D mesh are taken into account leaving aside the colorimetric ones. Yet, as confirmed in [5], colorimetric information plays an essential role in directing the visual attention of human observers while visualizing multimedia contents. This means that the degree of saliency of a region depends not only on its geometry but also on its colors.

The main contributions of the present paper can be resumed as follows: 1) The introduction of an innovative concept named Global Visual Saliency of a 3D colored mesh. 2) The use of the Dempster-Shafer Theory for combining the visual geometric and colorimetric saliency maps. This provides the Global Visual Saliency map of a 3D colored mesh. 3) The description and the availability of a constructed 3D colored mesh database used for testing the applications of the proposed Global Saliency.

To the best of our knowledge, the concept of Visual Global Saliency of a 3D colored mesh has never been proposed before. We define the Global Saliency map of a 3D colored mesh by the fusion result of its geometric and colorimetric saliency map. This Global Saliency map, more precise than a pure geometric or colorimetric map, due to the sensitivity of the HVS to both geometric and colorimetric features of a 3D content, associates a scalar reflecting the perceptual importance of each vertex. The paper is organized as follows. Section 2 presents the related works. Section 3 describes the proposed approach. In section 4, we present a new 3D colored mesh database used for the experimental tests. Section 5 presents the global saliency results of two colored meshes from the proposed database. In Section 6, we present two applications of our proposed approach and conclude in section

This work received funding from the Agence Nationale de la Recherche (ANR-14-CE27-0001 GRAPHSIP), and from the European Union FEDER/FSE 2014/2020 (GRAPHSIP project).

## II. RELATED WORK

Visual saliency estimation of 3D meshes is a new promising research area due to high potential applications. Until now, few methods were proposed in the state-of-the-art in comparison to the number of approaches computing visual saliency of 2D images. For example, we would find only one approach for the detection of colorimetric visual saliency of 3D meshes [6]. The rest of the state-of-the-art saliency estimation methods is dedicated to the geometry of the 3D mesh. Lee *et al.* [7] compute visual saliency of a 3D mesh by using a center-surround operator on Gaussian curvatures in a DoG (Difference Of Gaussians) scale space. Leifman *et al.* [1] define regions of interest by combining the distinctiveness of a vertex (using Spin-Images descriptor [8]) and extremities of the 3D mesh. Wu *et al.* [9] propose an approach that considers both the local contrast (multi-scale similarities between depths maps) and global rarity (based on a clustering of local features of local contrast). Song *et al.* [10] estimate saliency in the spectral domain by analyzing the deviation and features of the log-Laplacien spectrum. In [11], Tao *et al.* compute Zernike coefficients for patches obtained after an oversegmentation of the surface mesh. Then, after measuring the distinctness for each patch, the saliency proper to each patch is estimated based on its relevance to the most unsalient patches via manifold ranking.

All the methods presented above do not take into account the colorimetric features of the target 3D colored mesh. Therefore, in the next section, we present approaches generating two saliency maps (geometric and colorimetric) used in the proposed method for the computation of global saliency.

## III. GLOBAL SALIENCY OF 3D COLORED MESHES

Given a 3D object, our visual attention is placed on areas that present interesting geometric and colorimetric features of high degrees of saliency. To detect these regions, we compute a global saliency map obtained from the fusion of a geometric saliency map [2] and a RGB colorimetric saliency map [6] proposed in our previous works. These are based on two low level features of the HVS for the estimation of visual saliency that are the sensitivity to high contrast [12] and to strong discontinuities [13]. We present in this section the principal steps of these two approaches as well as the fusion process generating the final global saliency map.

### A. Notations

In the following, we represent a 3D mesh  $\mathcal{M}$  by a non-oriented graph  $\mathcal{G} = (\mathcal{V}, \mathcal{E})$  where  $\mathcal{V} = \{v_1, \dots, v_N\}$  is the set of  $N$  vertices and  $\mathcal{E} \subset \mathcal{V} \times \mathcal{V}$  the set of edges. The set of edges is deduced from the mesh faces that connect vertices. To each vertex  $v_i$  are associated its 3D coordinates  $\mathbf{p}_i = (x_i, y_i, z_i)^T \in \mathbb{R}^3$  that determine its position and a RGB color vector  $\mathbf{c}_i = (r_i, g_i, b_i)^T \in \mathbb{R}^3$ . The notation  $v_i \sim v_j$  is used to denote two adjacent vertices in  $\mathcal{G}$ .

### B. Geometric saliency map

It is commonly accepted that the human visual system is sensitive to large fluctuations surfaces [13]. Thereby, we consider that a vertex of the surface mesh is salient if it stands out from its surrounding and if its local geometric configuration is distinct from the one of its neighboring vertices. For this, we define our local patches of adaptive size that represent geometric surface descriptors.

We start by modeling the surface mesh by associating to each vertex  $v_i$  its vector representing the normal  $\mathbf{z}(v_i)$  and its two directional vectors  $\mathbf{x}(v_i)$  and  $\mathbf{y}(v_i)$  defining the 2D tangent plan  $\mathbf{P}(v_i)$  on  $v_i$ . For this, we compute a PCA at each vertex followed by an uniform orientation of the normal vectors [14]. In order to construct our local adaptive patches, we consider a spherical neighborhood  $S_\varepsilon(v_i)$  of ray  $\varepsilon$  around each vertex  $v_i$ . The vertices  $v_j$  belonging to the sphere  $S_\varepsilon$  are considered as neighbors of the target vertex  $v_i$  and are projected on the tangent plan  $\mathbf{P}(v_i)$ . Hence, 2D projected vectors  $\mathbf{v}'_i$  are obtained:

$$\mathbf{v}'_j = [(v_j - v_i).x(v_i), (v_j - v_i).y(v_i)]^T \quad (1)$$

It remains to precise the size of the patch. We propose patches of dynamic sizes obtained from the distance between the 2D coordinates of the projected vertices  $\mathbf{v}'_j$ . This will lead to patches defined on each vertex of different sizes depending on the local geometric configuration of the target vertex. The size of the patch of the target vertex  $v_i$  is defined along the  $x$  and  $y$  axis (respectively denoted  $T_x(\cdot)$  and  $T_y(\cdot)$ ) by:  $T_d(v_i) = \max_{(\mathbf{v}'_j, \mathbf{v}'_k) \in \mathbf{P}(v_i)} (\|\mathbf{v}'_j - \mathbf{v}'_k\|_2^2)$  where  $d$  is the  $x$  or  $y$  coordinate,  $\mathbf{v}'_j^d$  represents the coordinate  $d$  of the vector  $\mathbf{v}'_j$  and  $\|\cdot\|_2$  is the Euclidean norm. The constructed patch is then divided into a number of cells  $l \times l$ . This permits to get the index of the cell in which a vertex of the spherical neighborhood is projected. Finally, each cell of the patch  $P_i^k$  ( $k \in [1, l \times l]$ ) is filled with the absolute value of the sum of the projections heights:

$$\mathbf{H}(v_i) = \left( \sum_{\mathbf{v}'_j \in P_i^k} \|\mathbf{v}_j - \mathbf{v}'_j\|_2^2, \forall k \right)^T \quad (2)$$

where  $\mathbf{H}(v_i) \in \mathbb{R}^{l \times l}$  is the vector of cumulated heights in the cells of the patch.

Once the local descriptor is constructed, we compute the single-scale saliency of a target vertex  $v_i$  through a similarity measure between its associated patch and the patches associated to its neighboring vertices. This similarity is then affected to the weight of the edge  $(v_i, v_j) \in \mathcal{E}$  and is defined by:

$$w(v_i, v_j) = \exp \left[ - \frac{\kappa(v_j) * \|\mathbf{H}(v_i) - \mathbf{H}(v_j)\|_2^2}{\sigma(v_i) * \sigma(v_j) * \|\mathbf{v}_i - \mathbf{v}_j\|_2^2} \right] \text{ with } v_j \sim v_i \quad (3)$$

where  $\kappa(v_j)$  represents the curvature of the vertex  $v_j$  with the method described in [15],  $\|\mathbf{v}_i - \mathbf{v}_j\|_2$  represents the

Euclidean distance between the vertices  $v_i$  and  $v_j$  and  $\sigma(v_i)$  is a scale parameter defined by  $\sigma(v_i) = \max_{v_k \sim v_i} (\|\mathbf{v}_i - \mathbf{v}_k\|_2)$ .

Finally the single-scale saliency of the vertex  $v_i$  is defined by its mean degree:

$$\text{single-scale-saliency}(v_i) = \left( \frac{1}{|v_j \sim v_i|} \right) \sum_{v_i \sim v_j} w(v_i, v_j) \quad (4)$$

where  $|v_j \sim v_i|$  represents the cardinality of the adjacent neighborhood of  $v_i$  and  $w(v_i, v_j)$  is the weight of the edge  $(v_i, v_j)$ .

In order to enhance the precision of our saliency measure, we compute this latter on different scales. To do so, we vary the ray  $\varepsilon$  of the spherical neighborhood while constructing the local adaptive patches. This leads to three neighborhoods of rays  $\varepsilon$ ,  $2\varepsilon$  and  $3\varepsilon$  and therefore to three single-scale saliency geometric maps. These are combined using their respective entropies as weights. The multi-scale geometric saliency degree of a target vertex  $v_i$  is defined by:

$$\text{Multi-scale-geometric-saliency}(v_i) = \frac{\sum_{k=1}^3 \text{Single-scale-saliency}_k(v_i) * \text{entropy}_k}{\sum_{k=1}^3 \text{entropy}_k} \quad (5)$$

where  $k$  is the scale index.

### C. Colorimetric saliency map

To define the colorimetric measure of saliency, the RGB color vectors  $\mathbf{c}_i$  associated to vertices of the mesh will replace their geometric positions  $\mathbf{p}_i$  in the construction of the local adaptive patches process. Hence, a patch is constructed similarly to the patches necessary for the geometric map, however its cells  $P_i$  are filled with the mean RGB colors of the projected vertices  $\frac{1}{|c'_j \in P_i|} \sum_{c'_j \in P_i} \mathbf{c}'_j$  defining hence a

color vector  $\mathbf{C}(v_i)$  of the cumulated projections representing the local colorimetric patch on each vertex. We use a different similarity equation between the colorimetric patch of the target vertex  $v_i$  and the colorimetric patches of its neighboring vertices  $v_j$  that is affected to the weight of the edge  $(v_i, v_j) \in E$ :

$$w_C(v_i, v_j) = \exp \left[ - \frac{\|\mathbf{C}(v_i) - \mathbf{C}(v_j)\|_2^2}{\sigma_C(v_i) * \sigma_C(v_j) * l^2} \right] \quad (6)$$

where  $\sigma_C(v_i) = \max_{v_k \sim v_i} (\|\mathbf{c}_i - \mathbf{c}_k\|_2)$  and  $l$  is the cells number of the patch.

We define in the same previous manner the single-scale colorimetric saliency of a vertex  $v_i$  at the scale  $k$  by its mean degree:

$$\text{Single-scale-colorimetric-saliency}_k(v_i) = \frac{1}{|v_j \sim v_i|} \sum_{v_i \sim v_j} w_C(v_i, v_j) \quad (7)$$

and the multi-scale colorimetric saliency by:

$$\text{Multi-scale-colorimetric-saliency}(v_i) = \frac{\sum_{k=1}^3 \text{Single-scale-colorimetric-saliency}_k(v_i) * \text{entropy}_k}{\sum_{k=1}^3 \text{entropy}_k} \quad (8)$$

For more details about these visual saliency estimation approaches, please refer to [6] and [2].

### D. Fusion

1) *Preliminary*: Having the geometric and the RGB colorimetric saliency maps of a 3D colored mesh, the aim is to fuse them to obtain a global saliency map. We use for this purpose a part of the Dempster-Shafer Theory (DST) [16] to combine the two saliency maps considered as two independent sources. Dempster-Shafer Theory is based on the theory of probabilities that considers an upper and lower bounds. In the DST model, a discernment framework denoted as  $\Theta$  representing all possible hypotheses of a problem has to be defined. All subsets of the  $\Theta$  are included into a power set labelled as  $2^\Theta$ . Then a mass function  $m$  is defined and represents the belief allowed to the different states of the system. This function is defined from  $2^\Omega$  in  $[0, 1]$  as:

$$\sum_{A \subseteq \Omega} m(A) = 1 \quad \text{and} \quad m(\emptyset) = 0 \quad (9)$$

where  $m(A)$  represents a belief mass to  $A$ . Subsets having non-zero  $m(A)$  are called focal elements.

Given  $M$  mass functions  $m_1, m_2, \dots, m_M$  representing the information provided by  $M$  independent sources, these can be combined according to Dempster's rule:

$$(m_1 \oplus \dots \oplus m_M)(A) = \frac{1}{1 - K} \sum_{A_1 \cap \dots \cap A_M = A} \prod_{i=1}^M m_i(A_i) \quad (10)$$

where  $A_i \in 2^\Omega$ ,  $1 \leq i \leq M$  and  $K$  represents the conflict factor defined as:

$$K = \sum_{A_1 \cap \dots \cap A_M = \emptyset} \prod_{i=1}^M m_i(A_i) \quad (11)$$

$K$  is also known as the coefficient of discrepancy between the sources. The higher the value of  $K$ , the more incoherent the combination is.

One of the interesting implicit features of the DST is that the contribution of every subset is considered as single hypothesis. This simulates the reasoning logic of humans. Also, the DST fusion is characterized by its flexibility and its unsupervised aspect.

2) *Problem formulation*: In our case the framework discernment  $\Theta$  is represented by the set of vertices  $\mathcal{V}$  of the mesh. We define a subset of all the hypotheses as a fusion element. Hence, each vertex of the surface mesh is a single fusion element. We denote  $\epsilon$  the set of all fusion elements where  $\epsilon = \{v_1, \dots, v_N\}$  where  $N$  is the number of vertices of

the mesh.

As the saliency maps, we have obtained, associate a scalar representing the degree of saliency to each vertex, this degree can be considered as a probability of being salient for each element. Therefore, we consider the two saliency maps  $S_i$  (geometric and colorimetric) as two different sources in our DST model and use them to define the mass function  $m_i$  as:  $m_i(e) = S_i(e)$ ,  $e \in \epsilon$  where  $e$  represents a fusion element and  $1 \leq i \leq 2$ .

Finally, a probability value representing the global saliency degree of an element fusion is obtained by Eq. 10 with  $K$  fixed to 0.01.

#### IV. GREYC 3D COLORED MESH DATABASE

There is no available colored 3D mesh database in the literature that one may use to evaluate saliency detection algorithms that take into account colorimetric features. Therefore, we have constructed a colored mesh database using the *NextEngine* 3D color laser scanner. This latter is provided with a rotating plate and permits to acquire both geometric and colorimetric features of the 3D object. 15 object of different colors, textures and geometries were scanned leading to a reference corpus of 3D colored meshes. In addition, the database was enriched by applying several distortions to the reference 3D colored meshes. These distorted meshes are useful to evaluate the robustness and stability of a proposed approach detecting saliency. All the 3D meshes used in this paper belong to the Greyc 3D colored mesh database. For more details about the scanned objects, the process of acquisition and the used distortions, please refer to [17]. The database can be downloaded from <https://nouri.users.greyc.fr/ColoredMeshDatabase.html>.

#### V. GLOBAL SALIENCY RESULTS

##### A. Global saliency based on the RGB color space

Figure 1 presents a comparison between the geometric saliency map, the RGB colorimetric saliency map and the global saliency map of two 3D colored meshes. We can easily notice that there is a real difference between the three saliency maps. For the Dinosaur 3D mesh, the RGB colorimetric saliency map highlights details that haven't been detected in the geometric saliency map and vice versa (like the degraded colors on the back of the dinosaur or its forehead). Otherwise, the global saliency map combines the geometric and colorimetric features to better highlight the salient regions. This is visible at the level of the forehead which was judged as moderately salient on the geometric saliency map and as salient on the colorimetric map. However, on the global saliency map, the forehead is judged very salient because of the combination of the two saliencies. The same remarks can be made for the sides above the eyes, the long neck and the paw of the dinosaur.

For the Horse 3D mesh, this one contains many colors and contrasts. Hence, the colorimetric saliency map detects the majority of the salient regions. The Global Saliency map completes the latter at the level of regions that have strong

geometric fluctuations by adding salient regions highlighted on the geometric saliency map. This is visible at the level of the knees, the nose and the mouth of the mesh Horse.

We don't provide any comparison with state-of-the-art saliency methods insofar that there is currently no other view-independent approach that estimates the colorimetric or global saliency of a 3D colored mesh.

Evidently, an objective comparison between the obtained saliency results and a ground truth obtained from an eye tracker process will be more relevant. However, no ground truth associated to the colorimetric saliency of 3D colored meshes exists. This constitutes one aspect of our future work. Therefore, to complete our analysis of the proposed approach, we propose two applications of our Global Saliency model that attest its precision and relevance.

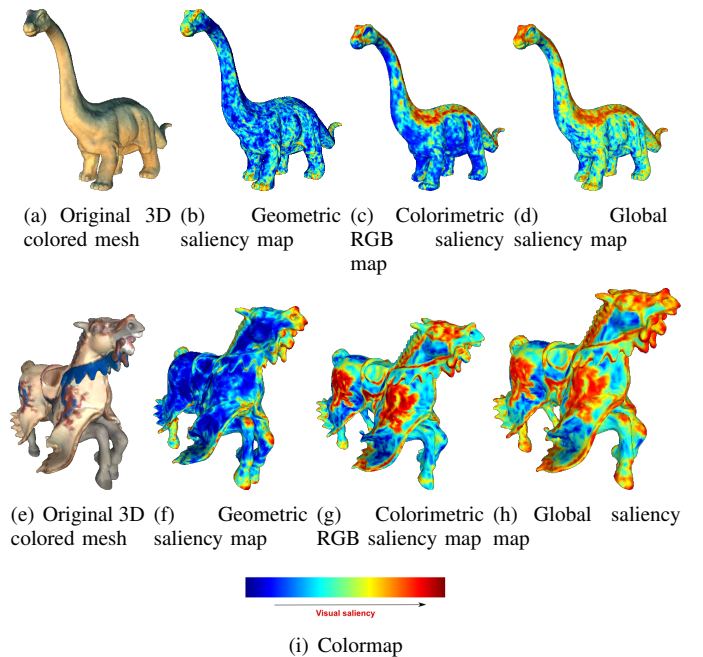


Fig. 1. Comparison between the global saliency map, the geometric saliency map and the RGB colorimetric saliency map.

##### B. Global saliency based on different colors spaces

It's not trivial to choose the adequate color space to use while treating colors, mainly when we are dealing with a specific application. We present in figure 2 the global saliency results where the associated colorimetric saliency maps are computed in the following color spaces: RGB, L\*a\*b, YUV, YCbCr, HSV and XYZ. We can notice that the global saliency results are somehow similar. There is no considerable difference between the obtained global saliency maps. Therefore, for complexity computation, we choose to compute visual colorimetric saliency in the RGB colorspace.

#### VI. APPLICATIONS OF THE GLOBAL VISUAL SALIENCY

For optimization purposes, the technologic advances relative to applications that need interactions with humans and particularly with their vision are increasingly taken into account

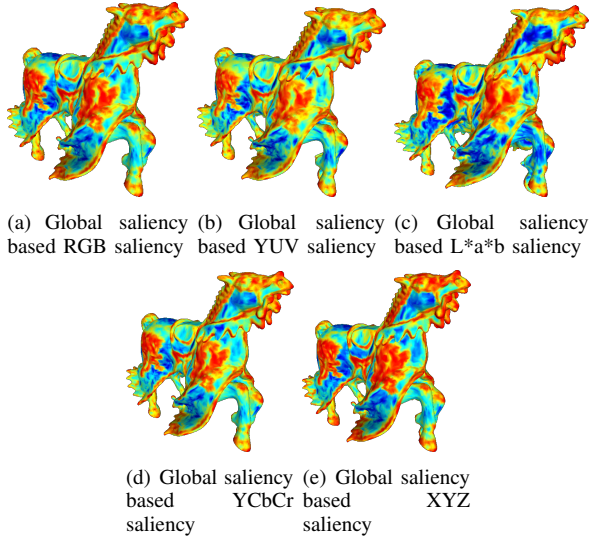


Fig. 2. Comparison between the global saliency maps where the colorimetric saliency maps are computed in different color spaces.

the limitations of the HVS. Selective visual attention represents an important mechanism in our perception. It permits an important time saving while visualizing the surrounding environment with the selection of potentially interesting informations while ignoring the rest. Therefore, saliency maps that can predict the regions on which the visual attention of the human observers will be focalized are the key for many applications. In this section, we present two applications that integrate our proposed global saliency map. These applications respond to the automatic optimal viewpoint selection and to the adaptive denoising of 3D colored meshes problems.

#### A. Optimal viewpoint selection of 3D colored meshes

The goal of the optimal viewpoint selection is to automatically select the most interesting viewpoint showing the maximum informations to the human observer. Few approaches have been proposed in the state-of-the-art that select the best viewpoint directly from the 3D structure [7] [1] [2] (this takes into account the depth and relief of the 3D model in contrary to 2D projections [18]). However all proposed approaches use only geometric saliency for the optimal selection of the viewpoint. We propose in this paper an extension of our previous viewpoint selecting approach [2] to 3D colored meshes. The principal criteria of this approach is to distinguish the viewpoint having the maximal global visual saliency. To do so, we begin by computing the global saliency map of a 3D mesh  $\mathcal{M}$  and select the viewpoint maximizing the global visual saliency along the  $x$  axis by sampling uniformly a sphere encompassing the 3D mesh. Let  $vp$  the viewpoint on the  $x$  axis and  $surface(vp)$  the set of vertices visible from  $vp$ . The saliency of this surface is defined by  $Saliency_{x-axis}(vp) = \sum_{v \in surface(vp)} Global - Saliency - map(v)$ . Hence, the optimal viewpoint along the  $x$  axis is defined by  $vp_x = \max(saliency_{x-axis})$  where  $vp_i$  represents the different viewpoints along the  $x$  axis. From  $vp_x$ , we proceed

similarly for selecting the optimal view point  $vp_y$  along the  $y$  axis. Once we have obtained  $vp_y$ , we search for the final optimal viewpoint using a gradient-descent along four axis at the same time:  $x, xy, (y - 45^\circ)$  and  $(y + 45^\circ)$ . Figure 3 presents a comparison between optimal viewpoints selected on a basis of a geometric saliency map and optimal viewpoints guided by a global saliency map. We can notice that optimal viewpoints selected with the use of our proposed global saliency map are more informative than the original viewpoints. These optimal viewpoints respond well to the criterion of the maximization of saliency and correspond to the most "natural" or likely views. However, the viewpoints selected with the use of the geometric saliency map don't expose the interesting features of the surface mesh. These generated viewpoints based-geometric saliency aren't natural for human observers.

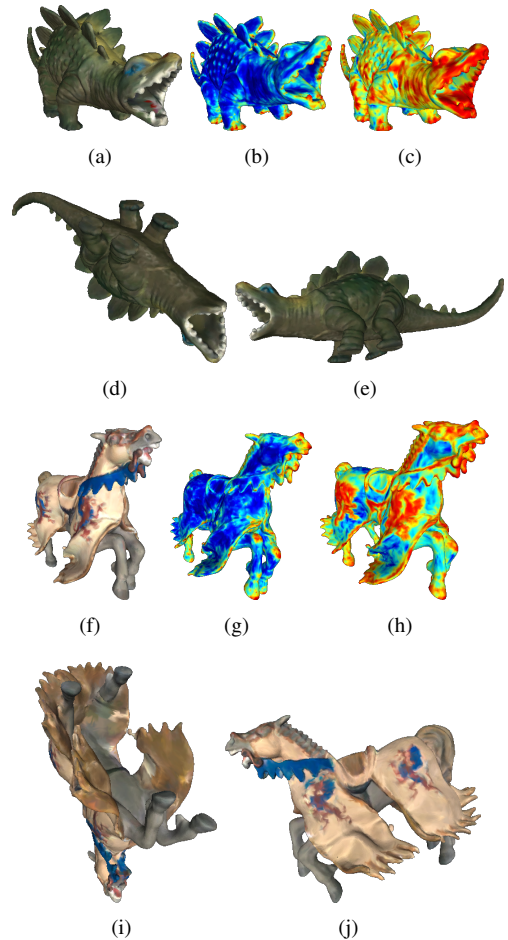


Fig. 3. Comparison between optimal viewpoints based-geometric saliency and optimal viewpoints based-global saliency. Images (a) and (f) refer to the original viewpoints of the two colored 3D meshes. Images (b) and (g) present their geometric saliency maps and images (c) and (h) their global saliency maps. Images (d) and (i) present the viewpoints based on geometric-based saliency of the two colored meshes. The viewpoints based on global saliency are presented in images (e) and (j).

#### B. Adaptive smoothing and denoising

In the field of mesh processing, smoothing and denoising play a significative role for noise reduction. Unfortunately, this process is usually accompanied with a loss of details that alter

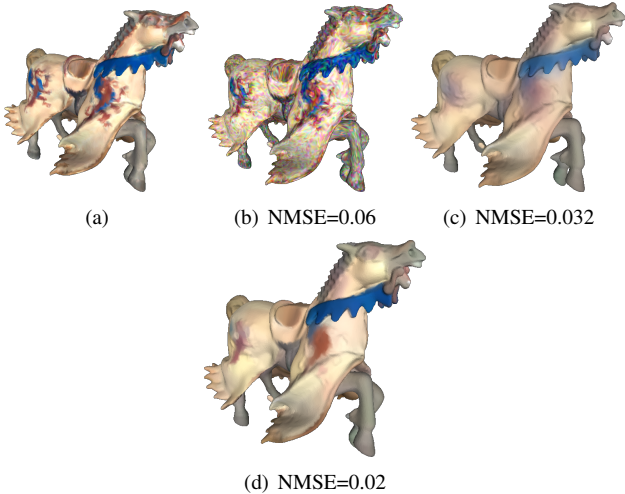


Fig. 4. Comparison between the results of the smoothing proposed in [19] and our adaptative smoothing based global saliency : (a) Noised Horse 3D colored mesh, (b) the denoising result of [19] and (c) our denoising result.

the visual rendering of the colored mesh. We propose in this section a modification of the diffusion process proposed in [19] operating an isotropic smoothing defined as:

$$\begin{cases} f^{(0)} = f \\ f^{(t+1)}(u) = \frac{\sum_{v \sim u} w(u,v) f^{(t)}(v)}{\sum_{v \sim u} w(u,v)} \quad \forall u \in V \end{cases} \quad (12)$$

where  $f$  is a function associating a set of RGB color vectors  $\mathbf{c}_i$  to vertices of the mesh  $\mathcal{M}$   $f : \mathcal{G} \rightarrow \mathcal{C} \subset \mathbb{R}^3$  and  $w(u, v)$  is the edge weight between the two vertices  $u$  and  $v$ .

In order to preserve details and salient features of the surface mesh while the smoothing process, we propose to modify the diffusion process of [19] with a global saliency weight as:

$$\begin{cases} f^{(0)} = f^0 \\ f^{(t+1)}(u) = \frac{\sum_{v \sim u} w(u,v) f^{(t)}(v) GS(u) GS(v)}{\sum_{v \sim u} w(u,v)} \quad \forall u \in V \end{cases} \quad (13)$$

where  $GS(u), GS(v)$  represent the global saliency of the vertices  $u$  and  $v$ .  $w(u, v)$  is a colorimetric similarity defined as  $w(u, v) = \exp\left(\frac{\|\mathbf{c}(v) - \mathbf{c}(u)\|_2^2}{\sigma_c(u)\sigma_c(v)}\right)$

where  $\sigma_c(v) = \max_{v \sim u} (\|\mathbf{c}_u - \mathbf{c}_v\|_2)$ . Figure 4 presents the results of denoising of a colored mesh affected by high Gaussian noise on its colors. We can notice that the result of denoising associated to our approach is of better visual quality compared to the results of [19]. The integration of global saliency has permitted to preserve the colorimetric details (like the contrast around the blue belt figure and the draws on the casing of horse). The low NMSE (Normalized Mean Square Error) confirms the good result associated to our approach in comparison to the approach of [19].

## VII. CONCLUSION

We have proposed an innovant approach for the estimation of global saliency that takes into account both geometric and

colorimetric features of a 3D colored mesh. This is done by combining two multi-scale saliency maps: geometric and RGB colorimetric maps. The global saliency map generated by our approach detects more salient regions in comparison to a purely geometric or colorimetric map since it takes into account both geometric and colorimetric features of the considered colored mesh. We have evaluated the precision and the contribution of our approach in two saliency-based applications and the results have showed the benefit of our proposed global saliency map. Future works will aim at constructing a ground truth saliency for an objective comparison of the proposed approach.

## REFERENCES

- [1] G. Leifman, E. Shtrom, and A. Tal, "Surface regions of interest for viewpoint selection," in *IEEE Conference on Computer Vision and Pattern Recognition*, 2012, pp. 414–421.
- [2] A. Nouri, C. Charrier, and O. L  zoray, "Multi-scale mesh saliency with local adaptive patches for viewpoint selection," *Signal Processing: Image Communication*, vol. 38, pp. 151–166, 2015.
- [3] P. Shilane and T. Funkhouser, "Distinctive regions of 3D surfaces," *ACM Transaction on Graphics*, vol. 26, no. 2, 2007.
- [4] L. Jinho, M. Baback, P. Hanspeter, and M. R. Machiraju, "Finding optimal views for 3D face shape modeling," in *Proc. International Conference on Automatic Face and Gesture Recognition*, 2004, pp. 31–36.
- [5] S. T. Shahrabaki, "Contribution de la couleur dans l'attention visuelle et un mod  le de saillance visuelle," Ph.D. dissertation, Universit   de Grenoble, 2015.
- [6] A. Nouri, C. Charrier, and O. L  zoray, "Multi-scale saliency of 3d colored meshes," in *International Conference on Image Processing (IEEE)*, 2015, pp. 2820–2824.
- [7] C. H. Lee, A. Varshney, and D. W. Jacobs, "Mesh saliency," *ACM Trans. Graph.*, vol. 24, no. 3, pp. 659–666, 2005.
- [8] A. E. Johnson and M. Hebert, "Using spin images for efficient object recognition in cluttered 3d scenes," *IEEE Transactions on Pattern Analysis and Machine Intelligence*, vol. 21, no. 5, pp. 433–449, 1999.
- [9] J. Wu, X. Shen, W. Zhu, and L. Liu, "Mesh saliency with global rarity," *Graphical Models*, vol. 75, no. 5, pp. 255 – 264, 2013.
- [10] R. Song, Y. Liu, R. R. Martin, and P. L. Rosin, "Mesh saliency via spectral processing," *ACM Transactions on Graphics*, vol. 33, no. 1, p. 6, 2014.
- [11] P. Tao, J. Cao, S. Li, X. Liu, and L. Liu, "Mesh saliency via ranking unsalient patches in a descriptor space," *Computers and Graphics*, vol. 46, pp. 264 – 274, 2015, shape Modeling International 2014. [Online]. Available: <http://www.sciencedirect.com/science/article/pii/S0097849314001113>
- [12] J. M. Wolf, "Guided search 2.0: A revised model of visual search," *Psychonomic Bulletin and Review*, vol. 1, no. 2, pp. 202 – 238, 1994.
- [13] S. Coren, L. M. Ward, and J. T. Enns, *Sensation and perception*. Wiley, 2003.
- [14] H. Hoppe, T. DeRose, T. Duchamp, J. McDonald, and W. Stuetzle, "Surface reconstruction from unorganized points," *SIGGRAPH Comput. Graph.*, vol. 26, no. 2, pp. 71–78, 1992.
- [15] S. Rusinkiewicz, "Estimating curvatures and their derivatives on triangle meshes," in *Proceedings of the 3D Data Processing, Visualization, and Transmission, 2Nd International Symposium*, ser. 3DPVT '04. IEEE Computer Society, 2004, pp. 486–493.
- [16] A. P. Dempster, "Upper and lower probabilities induced by a multivalued mapping," *Ann. Math. Statist.*, vol. 38, pp. 325–339, 1967.
- [17] A. Nouri, C. Charrier, and O. L  zoray, "Greyc colored mesh database," Greyc Laboratory, <https://tel.archives-ouvertes.fr/GREYC-IMAGE/hal-01441721v1>, Tech. Rep., 2017.
- [18] I. Howard, in *Seeing in depth*. University of Toronto Press, 2002.
- [19] A. Elmoataz, O. Lezoray, and S. Bougleux, "Nonlocal discrete regularization on weighted graphs: a framework for image and manifold processing," *IEEE transactions on Image Processing*, vol. 17, no. 7, pp. 1047–1060, 2008.